ACS APPLIED MATERIALS & INTERFACES

Research Article

www.acsami.org

Fabrication of Au@Pt Multibranched Nanoparticles and Their Application to In Situ SERS Monitoring

Qianling Cui,[#,‡,§,∥] Guizhi Shen,[#,⊥] Xuehai Yan,[⊥] Lidong Li,*[,‡] Helmuth Möhwald,[§] and Matias Bargheer*[,∥]

[‡]School of Materials Science and Engineering, University of Science and Technology Beijing, Beijing 100083, China

[⊥]Institute of Process Engineering, Chinese Academy of Sciences, Beijing 100190, China

[§]Max-Planck Institute of Colloids and Interfaces, Golm-Potsdam 14476, Germany

[∥]Institute of Physics and Astronomy, University of Potsdam, Potsdam 14476, Germany

Supporting Information

ABSTRACT: Here, we present an Au@Pt core−shell multibranched nanoparticle as a new substrate capable of in situ surface-enhanced Raman scattering (SERS), thereby enabling monitoring of the catalytic reaction on the active surface. By careful control of the amount of Pt deposited bimetallic Au@Pt, nanoparticles with moderate performance both for SERS and catalytic activity were obtained. The Pt-catalyzed reduction of 4-nitrothiophenol by borohydride was chosen as the model reaction. The intermediate during the reaction was captured and clearly identified via SERS spectroscopy. We established in situ SERS spectroscopy as a promising and powerful technique to investigate in situ reactions taking place in heterogeneous catalysis.

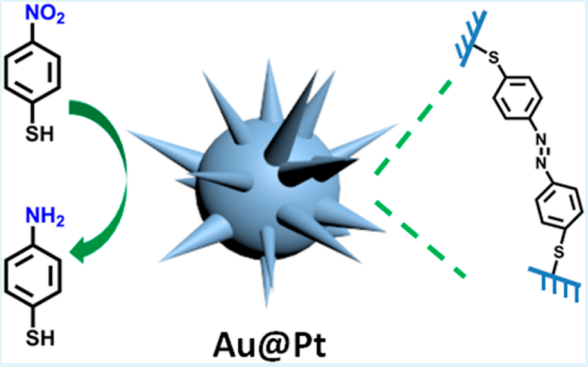

KEYWORDS: *nanoparticles, gold, core−shell nanostructure, surface-enhanced Raman scattering, heterogeneous catalysis, bimetallic nanoparticles*

INTRODUCTION

To investigate metal-catalyzed reactions, researchers have used several techniques, such as UV−vis absorption spectroscopy, infrared spectroscopy, and surface-enhanced Raman scattering (SERS) spectroscopy. Compared with the other two methods, SERS provides obvious advantages for monitoring the interfacial reaction. First, it can offer fingerprint vibrational information on the adsorbates on the surface, and the conversion of reactants, in addition, unstable reaction intermediates can be detected and identified. Second, the large enhancement factor of SERS, which is up to 1×10^{14}, takes the detection limit down to the level of single molecules.[1,2] Third, the Raman spectra of analytes rarely suffer from interference by the solvents present, including water, a common problem of infrared spectroscopy. In summary, SERS has become a versatile and powerful tool for in situ monitoring of metal-catalyzed chemical or electrochemical reactions at the nanoscale level.

Recently, more and more SERS-active substrates having catalytic action have been developed for in situ monitoring, providing new insights into the kinetics and mechanism of heterogeneous catalysis. Intrinsically strong Raman enhancement is observed for roughened surfaces of coinage metals (Ag, Au, and Cu) when the corrugations or nanoparticle deposits have a diameter greater than 20 nm. Catalytic action, however, typically occurs for these metal particles when their diameters are smaller than 10 nm, or on the surface of transition metals, e.g., Pd and Pt.[3] The Pt nanoparticles obtained by chemical reduction are mostly smaller than 10 nm, and it is difficult to acquire high Raman enhancement of targeted molecules adsorbed on these nanoparticles in nonelectrochemical environments.[4] It was reported that Pt nanoparticles with diameters up to 105 nm can be SERS-active, but the enhancement factor was quite low and the preparation required multistep seed-mediated growth under reflux condition.[5] A bifunctional platform can be obtained by integrating separate nanoparticles into a single entity through suitable methods of assembly.[6]

A much easier approach involves developing a core−shell nanostructure with a catalytic surface, where the SERS characteristics profits from the long-range electromagnetic field enhancement generated by the highly SERS-active inner core.[7−9] This strategy was employed to develop a variety of gold nanoparticles (AuNPs) with ultrathin shells of various transition metals, which showed good performance for in situ SERS monitoring of electrocatalytic reactions.[1,10,11] Bearing in

Received: July 18, 2014
Accepted: September 12, 2014
Published: September 12, 2014

mind that this borrowing of SERS activity decreases exponentially with distance from the inner core surface, the thickness of the surface coating has to be controlled carefully and restricted to only a few atomic layers. There was almost no SERS activity if a continuous and smooth shell of Pt was deposited on the large Au core, possibly because of the thickness being too high.[12] To address this issue, additional growth of Au protuberances was required to create some "hot spot" effects. A more versatile and simple strategy is still demanded to obtain bifunctional nanoparticles for the in situ SERS monitoring of plasmonic and catalytic properties.

Most of the above studies are limited to bimetallic nanoparticles with smooth surfaces.[13,14] However, using an anisotropic nanostructure with a rough surface is advantageous, both from the viewpoint of design of SERS-active systems as of catalysis. It is well-accepted that strong Raman enhancement is always observed on rough surface, which also provides a high surface area that is beneficial for catalysis. As a typical example, multibranched nanoparticles have become highly attractive in recent years.[15−21] Compared with spherical nanoparticles, the amount of exposed surface is increased owing to the multibranched nanostructure, as well as the number of atoms with low coordination, both factors leading to higher catalytic activity.[15,22−25]

In this contribution, Au@Pt nanoparticles with multibranched structures were readily prepared through the spontaneous deposition of Pt on the surface of gold multibranched nanoparticles under mild conditions. These bimetallic Au@Pt nanoparticles showed both excellent SERS characteristics and high catalytic activities. Both properties can be adjusted by careful control of the ratio of Pt to Au. For the first time we show their application to the in situ SERS monitoring of the model reaction the NO_2 reduction to NH_2 moieties by sodium borohydride in colloids.

EXPERIMENTAL SECTION

Materials. Chloroauric acid tetrahydrate ($HAuCl_4{\cdot}4H_2O$), chloroplatinic acid hexahydrate ($H_2PtCl_6{\cdot}6H_2O$), silver nitrate ($AgNO_3$), 4-nitrothiophenol (4-NTP), sodium borohydride ($NaBH_4$), and ascorbic acid were purchased from Sigma-Aldrich. All chemical reagents were used as received without further purification. Ultrapure Millipore water (18.6 MΩ·cm) was used throughout the experiments.

Preparation of Au@Pt Multibranched Nanoparticles. Two hundred microliters of 10 mM aqueous $HAuCl_4$ solution was mixed with 10 mL of water, then 30 μL of 10 mM aqueous $AgNO_3$ solution was added. After the solutions were thoroughly mixed, 40 μL of 100 mM ascorbic acid was quickly added, and the mixture was stirred vigorously for 20 s at room temperature. After purification through several centrifugations under a speed of 5000 rpm for 10 min, the gold nanoparticles were dispersed in 10 mL of water. For the following growth of the Pt shell, 50, 100, 150, 200, and 250 μL of 10 mM aqueous H_2PtCl_6 solution was added, respectively, into 10 mL of AuM colloids under stirring, followed by addition of 40 μL of 100 mM ascorbic acid. The color of the mixture changed from blue to dark gray, and it was kept at room temperature for 1 h. The nanoparticles were then collected and washed thoroughly with water by several centrifugations at a speed of 5000 rpm for 10 min. The products obtained were denoted as Au@Pt-1, Au@Pt-2, Au@Pt-3, Au@Pt-4, Au@Pt-5, respectively,

In Situ Monitoring of the Catalytic Reaction with SERS. Ten microliters of 10 mM 4-NTP in ethanol solution was added to 1 mL of colloidal suspension of Au@Pt NPs and incubated at room temperature. To remove free 4-NTP the NPs were washed with water and resuspended in 500 μL of H_2O. 100 μL of 20 mM $NaBH_4$ solution was added to this mixture to start the catalytic reaction. SERS spectra were collected directly from the colloidal suspension after different reaction times.

Characterization. Transmission electron microscopy (TEM), high-resolution TEM (HRTEM), and TEM-EDS mapping were performed with a JEOL JEM-2100 transmission electron microscope, equipped with an energy-dispersive X-ray spectrometer (EDS, Horiba EMAX Energy EX-350) operated at an acceleration voltage of 200 kV. Extinction and absorption spectra were recorded on a Cary 500 Scan UV−vis−near-infrared (UV−vis−NIR) spectrophotometer. Scanning electron microscopy (SEM) measurements were performed using a Philips XL30 electron microscope at an accelerating voltage of 3 kV. The X-ray diffraction (XRD) patterns were recorded using a Bruker D8 Advance X-ray diffractometer. The particle size and size distributions were measured by a ZetaSizer Nano ZS (Malvern Instruments). The Raman spectra were obtained using a confocal Raman microscope (alpha 300, WITec, Ulm, Germany) equipped with laser excitation at a wavelength of 785 nm (I_2 laser). The laser beam was focused through a 60× water immersion (Nikon, NA=1.0) microscope objective. The SERS spectra were acquired with a thermoelectrically cooled CCD detector (DU401A-BV, Andor, UK) placed behind the spectrometer (UHTS 300; WITec, Ulm, Germany) with a spectral resolution of 3 cm^{-1}. The diameter of the laser spot area is about 1 μm, and the penetration depth is about 25 μm. The Raman band of a silicon wafer at 520 cm^{-1} was used to calibrate the spectrometer.

RESULTS AND DISCUSSION

In this work, Au@Pt multibranched nanoparticles were synthesized in aqueous solution through a simple two-step procedure taking place at room temperature, in contrast to the procedures reported elsewhere that involved the reaction under reflux condition.[12] Gold multibranched (AuM) nanoparticles with large sizes were chosen as the core for growth of the Pt shell. The hot spots formed in the gaps between neighboring tips and the planar gold surface ensures they can provide the required high SERS activity.[26,27] The preparation of AuMs was similar to the procedure using gold nanostars as reported by Cheng,[28] with a minor modification. The synthesis was realized in a facile way, where $HAuCl_4$, $AgNO_3$, and ascorbic acid were used as gold precursor, structure directing agent, and reducing agent, respectively. The presence of Ag ions induced the anisotropic growth of gold, and increased the formation of branches on the surface. The as-prepared AuM acted a template for the growth of the Pt shell, brought about by the addition of H_2PtCl_6 and ascorbic acid under stirring at ambient temperature. The continuous growth of the Pt shell is a result of combination of galvanic replacement and reagent reduction. Images a and e in Figure 1 show TEM and SEM images of the AuM nanoparticles, respectively, where many tips on the gold surface are seen. These nanoparticles are quite uniform, with an average size of about 90 nm. The HRTEM image of individual AuM (Figure 1c) reveals that the *d*-spacings of adjacent fringes are 2.35 ± 0.03 Å, corresponding to the (111) planes of face-centered cubic (fcc) Au. EDS spectroscopy (Figure 1g) of the AuMs confirms the presence of Au together with trace amounts of Ag. Images b and f in Figure 1 show the TEM and SEM images of the Au@Pt nanoparticles, respectively, taking Au@Pt-3 as a typical example. It can be clearly seen that the nanoparticles possess three-dimensional dendritic nanostructure, with an enlarged size compared with the AuM cores. The HRTEM result (Figure 1d) shows that the *d*-spacings of adjacent fringes are 2.25 ± 0.03 Å, ascribed to the (111) planes of Pt. The elemental composition was determined by EDS analysis (Figure 1h), where the presence of a Pt peak proves the successful incorporation of Pt into the structure. The mapping

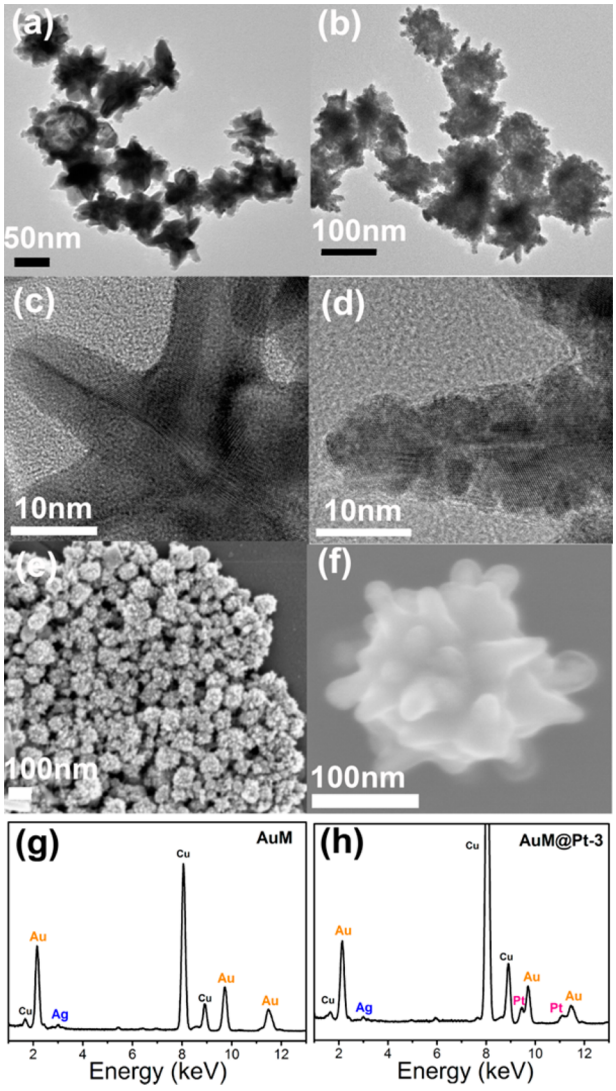

Figure 1. (a) TEM, (c) HRTEM, (e) SEM images, and (g) EDS analysis of the gold multibranched nanoparticles (AuM NPs); (b) TEM, (d) HRTEM, (f) SEM images, and (h) EDS analysis of the Au@Pt multibranched nanoparticles (Au@Pt-3).

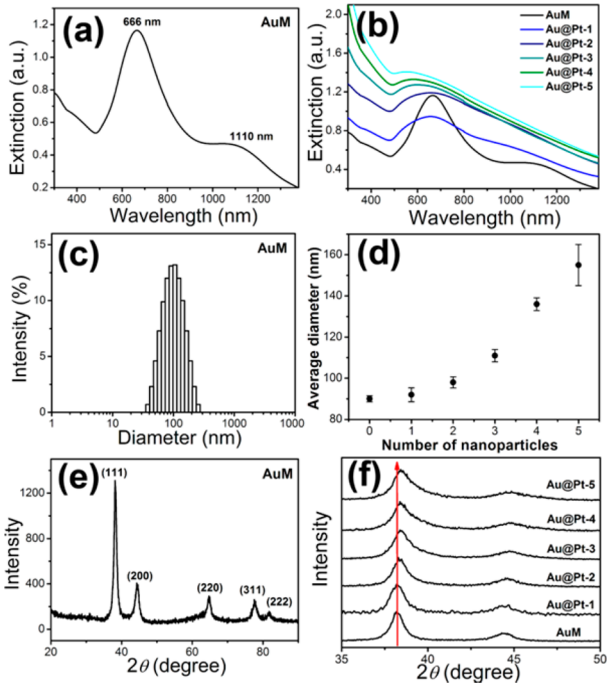

Figure 2. Extinction spectra of (a) AuM and (b) Au@Pt NPs; (c) size distributions of AuM NPs and (d) average sizes of Au@Pt NPs; (e) XRD patterns of AuM and (f) Au@Pt nanoparticles.

image of different elements of Au@Pt-3 (Figure S1) shows that most of the Pt distribute outside the Au core, confirming their core−shell structures.

The extinction spectrum of AuMs (Figure 2a) shows two distinct surface plasmon resonance (SPR) bands at 666 and 1110 nm. Compared with gold nanostars, the second band of AuM shifted to longer wavelengths owing to the increased number and aspect ratio of protrusions on the surface.[28,29] After Pt growth on the sample, both SPR bands broadened and shifted to shorter wavelengths (Figure 2b), indicating the successful deposition of Pt. The SPR peak of gold can still be observed even after it is covered with many Pt nanobranches, proving that these Pt nanobranches are noncompact.[25] This is an important aspect in order to maintain a strong electromagnetic field for SERS monitoring.[30] A narrow size distribution of AuM colloids with an average diameter of about 90 nm is demonstrated in Figure 2c. The sizes of Au@Pt NPs increase from 92 to 155 nm as the fraction of Pt is increased (Figure 2d), which clearly shows the successful control of particle size through a change in the Pt concentration during the growth on AuM. The X-ray diffraction (XRD) peaks of AuM (Figure 2e) are assigned to the (111), (200), (220), (311), and (222) planes of Au. After the growth of Pt branches on the surface, the diffraction peaks are broadened and shift gradually (Figure 2f). The (111) reflection shifts from 38.2 to 38.5 degree, although for pure Pt it is expected at 40°. The thickest Pt shell shows a shoulder of the peak at this position. These data suggest that Pt diffuses into the AuM, and that the Pt layer contains Au.

The catalytic activity of the metal nanoparticles was frequently checked by the reduction of an aromatic nitro compound to its corresponding amino derivate, a reaction which can easily be monitored by UV−vis spectroscopy.[31] We also believe these bimetallic nanoparticles show catalytic activity toward other reactions, which can be catalyzed by Pt. The reduction of 4-nitrothiolphenol (4-NTP) in the presence of these nanoparticles was used to compare the catalytic activity of catalysts with different Pt content. The initial concentrations of 4-NTP and $NaBH_4$ were 0.1 and 10 mM, respectively, so that $NaBH_4$ was present in large excess. Figure 3b shows the absorption spectra of 4-NTP with $NaBH_4$ using AuM nanoparticles as catalyst, initially and after 3 h. The absorption peak at about 410 nm shows no obvious change, indicating that no reaction takes place using AuM as a catalyst in the absence of Pt. Obviously, AuM nanoparticles are inefficient catalysts for the reduction of 4-NTP, which can be explained by the molecular orientation on their surfaces. Owing to the high affinity of the thiol group for gold, the 4-NTP molecules form a dense monolayer on the gold surface via an end-on orientation. The NO_2 groups are far away from the gold surface, which serves as the electron relay between the adsorbed reactant and the borohydride.[32,33] Consequently, the charge transfer between metal and NO_2 groups, that favors the efficient evolution of the catalytic reaction, cannot occur. To resolve this issue, Pt, a more efficient catalyst, is required, introduced as an

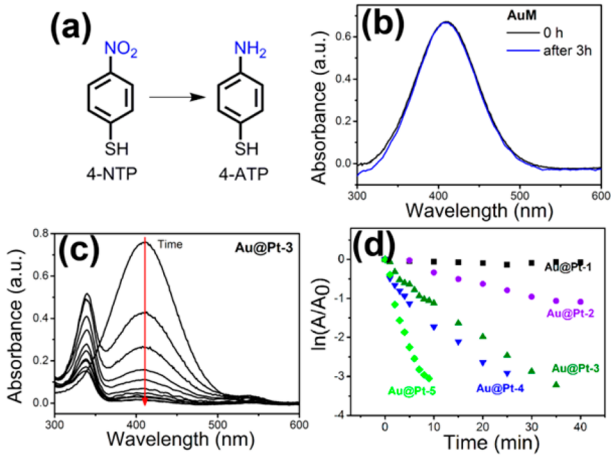

Figure 3. (a) Chemical structure of 4-nitrothiophenol (4-NTP) and of the corresponding reduction product, 4-aminothiophenol (4-ATP). (b) Absorption spectra of 4-NTP with $NaBH_4$ in the presence of AuM before and after 3 h. (c) Absorption spectra of 4-NTP with $NaBH_4$ in the presence of Au@Pt-3 nanoparticles with time up to 50 min. The time interval between each curve is 5 min. (d) Plots of $\ln(A/A_0)$ of 4-NTP as a function of time for the reaction catalyzed by Au@Pt nanoparticles with different thickness of the Pt shell.

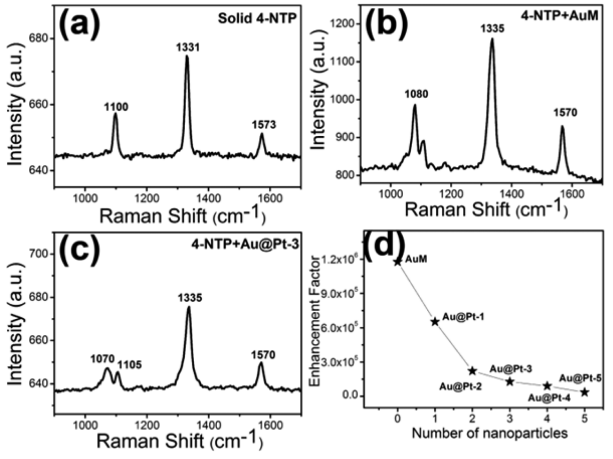

Figure 4. (a) Raman spectrum of solid 4-NTP, (b) SERS spectrum of 4-NTP in AuM colloids, (c) SERS spectrum of 4-NTP in Au@Pt-3 colloids, (d) calculated enhancement factors of Au@Pt nanoparticles with different thickness of the Pt shell.

outerlayer to increase the catalytic activity. Hence the reduction reactions of 4-NTP catalyzed by Au@Pt nanoparticles with different Pt contents were investigated. As an example, the absorption spectra change with reaction duration in the presence of Au@Pt-3 nanoparticles (Figure 3c). The characteristic peak of 4-nitrothiophenolate at 410 nm decreases with increasing reaction time, and nearly disappears after 30 min. Instead, a new peak around 340 nm assigned to the product, 4-aminothiophenol (4-ATP) is observed as expected. To compare the catalytic activities of the Au@Pt with different Pt contents, $\ln(A/A_0)$ is plotted as a function of reaction time (Figure 3d), where A and A_0 are the relative concentrations of 4-NTP at time $t = t$ and $t = 0$, respectively. Clearly, the catalytic activity of the bimetallic nanoparticles is enhanced as the Pt content increases. This is reasonable because the defects in the bimetallic nanoparticles increased as the Pt amount increased in the galvanic reaction. They provide more active sites for the catalysis reaction. It is noted that although the concentration of $NaBH_4$ is in large excess compared with 4-NTP, the nonlinear relationships show that the reaction does not follow pseudo-first order kinetics. This contrasts with the catalytic behavior of small Pt nanoparticles.[31] To understand this behavior, SERS was used, because this technique has been demonstrated to be a promising surface analysis tool to investigate the structural evolution of molecules participating in heterogeneous catalysis.

Previous studies demonstrated that 4-NTP molecules on bare SERS-active substrates (Au, Ag) are converted by plasmon-driven dimerization of the azo compound, p,p′-dimercaptoazobenzene (DMAB) under high power laser irradiation. This chemical transformation showed a direct dependence on the laser power, the substrate and the irradiation time.[34−37] To avoid this unwanted side reaction, a lower laser power of 0.2 mW was used for the Raman measurements. Figure 4a shows the normal Raman spectrum of solid 4-NTP in the range 900−1700 cm^{-1}. It exhibits the characteristic bands of 4-NTP at 1100, 1331, and 1573 cm^{-1}, assigned to the C−H bending, NO_2 symmetric stretching, and C═C stretching modes, respectively.[38] For comparison the SERS spectrum of 4-NTP adsorbed on AuM surfaces is nearly the same as the normal Raman spectrum of pure 4-NTP (Figure 4b), except for a small SERS band at 1080 cm^{-1} assigned to the vibrational mode of C−H.[34] The SERS spectrum of 4-NTP in the presence of Au@Pt-3 nanoparticles is similar to that obtained with AuM, but with decreased Raman intensity (Figure 4c). Such a decline in Raman enhancement can be explained by the fact that the electromagnetic field of the inner Au core decays nearly exponentially with the distance from the metal surface. The enhancement factors of each nanoparticles were calculated out based on the Raman intensities of the characteristic NO_2 group at 1336 cm^{-1}, according to the calculation method in previous work.[39] The calculated values are displayed in Figure 4d. The bare gold nanoparticles AuM display the largest enhancement factor of 1.2×10^6, and this value decreases as the Pt content increases. This is reasonable because it is well accepted that the presence of Pt has a negative effect on SERS performance of AuM and the increased Pt shell enlarges the distance toward the SERS-active Au core. The Raman signal of the targeted molecules are still clearly observable even on the Au@Pt-5 sample, where the Pt shell is sufficiently thick to screen the electromagnetic field of the inner SERS-active core. This Raman enhancement is presumably caused by the multibranched structure of the colloids.

The plasmon-driven chemical dimerization of 4-NTP to DMAB can also take place under continuous exposure to the laser for extended periods, even at low power levels.[35,36] Therefore, the stabilities of 4-NTP molecules on the AuM and Au@Pt-3 surface were investigated by illuminating the samples continuously under the laser beam with a fixed power of 0.2 mW. After 30 min, the new bands in region A and B (Figure 5a) indicate that a small portion of 4-NTP on the bare gold surface was dimerized into DMAB by a surface-catalyzed chemical reaction (Figure 5). The Raman spectra of 4-NTP molecules on the Au@Pt-3 surface are nearly unchanged within a 1 h period, implying that the side reaction does not occur. It can be reasonably concluded that 4-NTP was barely subjected to the plasmon-driven surface catalytic reaction on Pt compared with the case with gold, a finding that is consistent with the observations of Kim et al.[5]

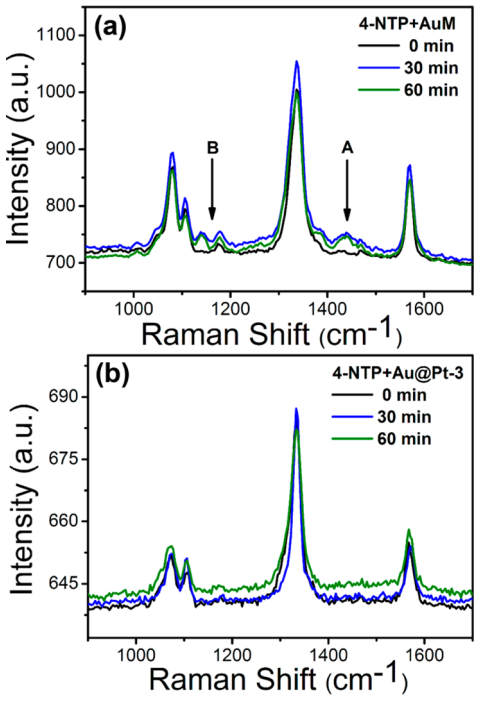

Figure 5. Raman spectra of 4-NTP molecules in (a) AuM colloids and (b) Au@Pt-3 colloids under continuous laser irradiation for various times.

All Au@Pt NPs exhibited both catalytic and SERS activities and this enables the in situ SERS monitoring of the surface catalytic reaction. Here, Au@Pt-3 was chosen as a representative catalyst, in view of its moderate activity in both catalysis and SERS. The SERS spectra taken during the reduction of 4-NTP in the presence of $NaBH_4$, catalyzed by Au@Pt-3, are shown in Figure 6. The strong Raman band at 1336 cm^{-1}

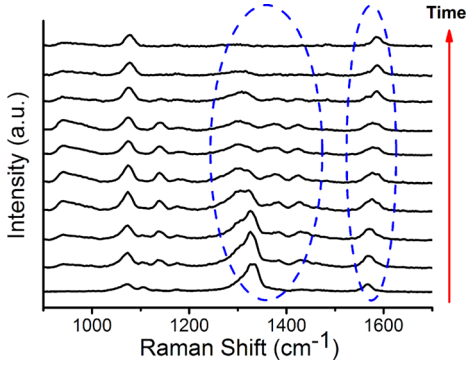

Figure 6. SERS spectra recorded during the reduction of 4-NTP on Au@Pt-3 colloids after different reaction times. From bottom to top: SERS spectra recorded at 0, 5, 10, 15, 20, 25, 30, 35, 40, and 45 min after addition of $NaBH_4$ solution. The spectra are offset for clarity.

gradually decreases and disappears after 45 min, indicating that the NO_2 groups are completely reduced. The band arising from the phenyl ring modes of 4-NTP at 1570 cm^{-1} also decreases gradually with a concomitant increase in intensity of a new band at 1588 cm^{-1}, assigned to the phenyl ring modes of the 4-ATP product. The Raman spectrum of the final product is consistent with that reported for 4-ATP.

The UV–vis absorption spectra show an additional peak at 540 nm, emerging unexpectedly after the reaction begins and disappearing by the time the reaction ends. This implies that a new intermediate species is formed during the reaction. It is difficult to gain more information about this species from the UV–vis absorption spectra alone. SERS spectra can, however, reflect the fingerprint vibration of molecules adsorbed at the interface, thereby providing useful structural information. One typical Raman spectrum observed during the reduction reaction is shown in Figure 7b. In addition to the Raman signals of 4-

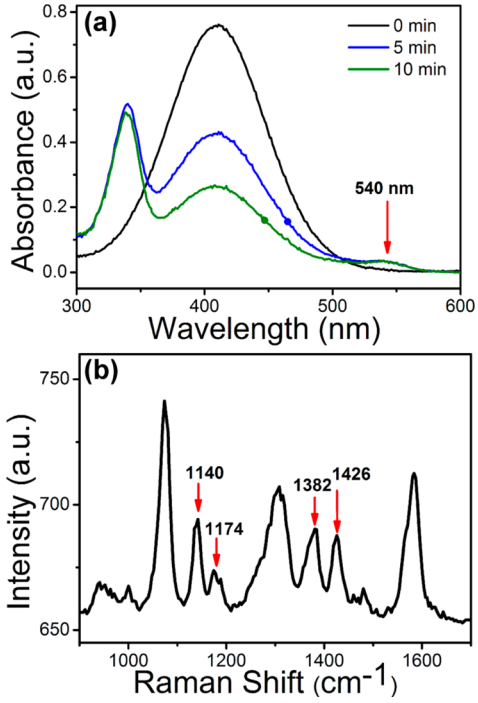

Figure 7. (a) UV–vis absorption spectra of the mixture of 4-NTP, $NaBH_4$ and Au@Pt-3, after different reaction times. (b) Raman spectrum of the intermediate during the reduction reaction of 4-NTP catalyzed by Au@Pt-3.

NTP and 4-ATP, some new bands due to DMAB are observed, so this entity clearly coexists in the system.[12,37,40] The bands at 1382 and 1426 cm^{-1} are caused by the N=N stretching vibration modes of DMAB, while the peak at 1140 cm^{-1} is related to the C–N symmetric stretching mode. Since there were no spectral changes in previous experiments (Figure 5b), a plasmon-driven chemical conversion of 4-NTP to DMAB can be excluded. It was also reported that the plasmon-driven dimerization of the product, 4-ATP molecules, also could generate DMAB.[37] To exclude this interfere, the SERS spectrum of 4-ATP on Au@Pt-3 was also examined and shown in Figure S2, where no obvious Raman peaks of DMAB molecules was observed. Furthermore, the laser beam was switched off in order to minimize laser-induced formation of DMAB during the collecting interval. It is safe to conclude that DMAB is indeed generated from the Pt-catalyzed reduction reaction as an intermediate, as was also reported by others.[12] In catalysis, it is well-accepted that the metallic surface serves as the electron relay between the adsorbed reactant and borohydride. Borohydride ions that adsorbed on the metallic surface accept an electron donated by metal, and then generate a surface-hydrogen species. However, 4-NTP molecules adopt the stand-up orientation on the metallic surface through the affinity anchoring thiol group, with nitro groups far away from the catalytic surface. In this case, the nitro groups cannot

contact with the surface-hydrogen species and the catalytic reaction would not take place. If the dimerization reaction occurs, the azo bonds would get close to the catalytically active surface, and the catalysis reaction will proceed smoothly.

CONCLUSIONS

This work presents a facile and economical way toward the large-scale synthesis of Au@Pt multibranched nanoparticles. These bimetallic nanoparticles exhibit both catalytic action and SERS activity. Platinum deposited on gold multibranched nanoparticles shows high catalytic activity for the reduction of 4-NTP to 4-ATP. As the Pt content is increased, catalytic activity increases, while the SERS activity declines. The Raman signals are still clear enough for quantification even if the Pt shell is much thicker than a monolayer, due to the large and rough surface of the particles. The reduction of 4-NTP to 4-ATP catalyzed by Au@Pt nanoparticles can be monitored complementarily by UV−vis absorption and SERS methods. Since the plasmon-driven side reaction does not occur under extremely low laser power, the DMAB molecules, that appear during the reaction, are intermediates in the reduction reaction that can thus be studied in further detail.

ASSOCIATED CONTENT

Supporting Information

The authors declare no competing financial interest. This material is available free of charge via the Internet at http://pubs.acs.org.

AUTHOR INFORMATION

Corresponding Authors

*E-mail: bargheer@uni-potsdam.de.
*E-mail: lidong@mater.ustb.edu.cn.

Author Contributions

#Q.C. and G.S. contributed equally to this study.

Notes

The authors declare no competing financial interest.

ACKNOWLEDGMENTS

The authors gratefully acknowledge Xiaofeng Liu (Max Planck Institute of Colloids and Interfaces, Germany) for his kind support with the XRD measurements.

REFERENCES

(1) Tian, Z. Q.; Ren, B.; Li, J. F.; Yang, Z. L. Expanding Generality of Surface-Enhanced Raman Spectroscopy with Borrowing SERS Activity Strategy. *Chem. Commun.* **2007**, 3514−3534.
(2) Nie, S. M.; Emery, S. R. Probing Single Molecules and Single Nanoparticles by Surface-Enhanced Raman Scattering. *Science* **1997**, *275*, 1102−1106.
(3) Ahmadi, T. S.; Wang, Z. L.; Green, T. C.; Henglein, A.; El-Sayed, M. A. Shape-Controlled Synthesis of Colloidal Platinum Nanoparticles. *Science* **1996**, *272*, 1924−1925.
(4) Abdelsalam, M. E.; Mahajan, S.; Bartlett, P. N.; Baumberg, J. J.; Russell, A. E. SERS at Structured Palladium and Platinum Surfaces. *J. Am. Chem. Soc.* **2007**, *129*, 7399−7406.
(5) Kim, K.; Kim, K. L.; Lee, H. B.; Shin, K. S. Surface-Enhanced Raman Scattering on Aggregates of Platinum Nanoparticles with Definite Size. *J. Phys. Chem. C* **2010**, *114*, 18679−18685.
(6) Joseph, V.; Engelbrekt, C.; Zhang, J. D.; Gernert, U.; Ulstrup, J.; Kneipp, J. Characterizing the Kinetics of Nanoparticle-Catalyzed Reactions by Surface-Enhanced Raman Scattering. *Angew. Chem., Int. Ed.* **2012**, *51*, 7592−7596.
(7) Khanal, B. P.; Zubarev, E. R. Polymer-Functionalized Platinum-On-Gold Bimetallic Nanorods. *Angew. Chem., Int. Ed.* **2009**, *48*, 6888−6891.
(8) Chantry, R. L.; Atanasov, I.; Siriwatcharapiboon, W.; Khanal, B. P.; Zubarev, E. R.; Horswell, S. L.; Johnston, R. L.; Li, Z. Y. An Atomistic View of the Interfacial Structures of AuRh and AuPd Nanorods. *Nanoscale* **2013**, *5*, 7452−7457.
(9) Liu, R.; Liu, J. F.; Zhang, Z. M.; Zhang, L. Q.; Sun, J. F.; Sun, M. T.; Jiang, G. B. Submonolayer-Pt-Coated Ultrathin Au Nanowires and Their Self-Organized Nanoporous Film: SERS and Catalysis Active Substrates for Operando SERS Monitoring of Catalytic Reactions. *J. Phys. Chem. Lett.* **2014**, *5*, 969−975.
(10) Tian, Z. Q.; Yang, Z. L.; Ren, B.; Li, J. F.; Zhang, Y.; Lin, X. F.; Hu, J. W.; Wu, D. Y. Surface-Enhanced Raman Scattering from Transition Metals with Special Surface Morphology and Nanoparticle Shape. *Faraday Discuss.* **2006**, *132*, 159−170.
(11) Li, J. F.; Tian, X. D.; Li, S. B.; Anema, J. R.; Yang, Z. L.; Ding, Y.; Wu, Y. F.; Zeng, Y. M.; Chen, Q. Z.; Ren, B.; Wang, Z. L.; Tian, Z. Q. Surface Analysis using Shell-Isolated Nanoparticle-Enhanced Raman Spectroscopy. *Nat. Protoc.* **2013**, *8*, 52−65.
(12) Xie, W.; Herrmann, C.; Kompe, K.; Haase, M.; Schlucker, S. Synthesis of Bifunctional Au/Pt/Au Core/Shell Nanoraspberries for in Situ SERS Monitoring of Platinum-Catalyzed Reactions. *J. Am. Chem. Soc.* **2011**, *133*, 19302−19305.
(13) Du, B. C.; Tong, Y. Y. A Coverage-Dependent Study of Pt Spontaneously Deposited onto Au and Ru Surfaces: Direct Experimental Evidence of the Ensemble Effect for Methanol Electro-Oxidation on Pt. *J. Phys. Chem. B* **2005**, *109*, 17775−177780.
(14) Park, I. S.; Lee, K. S.; Choi, J. H.; Park, H. Y.; Sung, Y. E. Surface Structure of Pt-Modified Au Nanoparticles and Electrocatalytic Activity in Formic Acid Electro-Oxidation. *J. Phys. Chem. C* **2007**, *111*, 19126−19133.
(15) Lim, B.; Xia, Y. N. Metal Nanocrystals with Highly Branched Morphologies. *Angew. Chem., Int. Ed.* **2011**, *50*, 76−85.
(16) Teng, X. W.; Liang, X. Y.; Maksimuk, S.; Yang, H. Synthesis of Porous Platinum Nanoparticles. *Small* **2006**, *2*, 249−253.
(17) Guo, S. J.; Wang, L.; Dong, S. J.; Wang, E. K. A Novel Urchinlike Gold/Platinum Hybrid Nanocatalyst with Controlled Size. *J. Phys. Chem. C* **2008**, *112*, 13510−13515.
(18) Sun, S. H.; Yang, D. Q.; Villers, D.; Zhang, G. X.; Sacher, E.; Dodelet, J. P. Template- and Surfactant-free Room Temperature Synthesis of Self-Assembled 3D Pt Nanoflowers from Single-Crystal Nanowires. *Adv. Mater.* **2008**, *20*, 571−574.
(19) Mahmoud, M. A.; Tabor, C. E.; El-Sayed, M. A.; Ding, Y.; Wang, Z. L. A New Catalytically Active Colloidal Platinum Nanocatalyst: The Multiarmed Nanostar Single Crystal. *J. Am. Chem. Soc.* **2008**, *130*, 4590−4591.
(20) Senyuk, B.; Evans, J. S.; Ackerman, P. J.; Lee, T.; Manna, P.; Vigderman, L.; Zubarev, E. R.; van de Lagemaat, J.; Smalyukh, I. I. Shape-Dependent Oriented Trapping and Scaffolding of Plasmonic Nanoparticles by Topological Defects for Self-Assembly of Colloidal Dimers in Liquid Crystals. *Nano Lett.* **2012**, *12*, 955−963.
(21) Vigderman, L.; Zubarev, E. R. Starfruit-Shaped Gold Nanorods and Nanowires: Synthesis and SERS Characterization. *Langmuir* **2012**, *28*, 9034−9040.
(22) Sanlés-Sobrido, M.; Pérez-Lorenzo, M.; Rodríguez-González, B.; Salgueiriño, V.; Correa-Duarte, M. A. Highly Active Nanoreactors: Nanomaterial Encapsulation Based on Confined Catalysis. *Angew. Chem., Int. Ed.* **2012**, *51*, 3877−3882.
(23) Sanles-Sobrido, M.; Correa-Duarte, M. A.; Carregal-Romero, S.; Rodríguez-González, B.; Álvarez-Puebla, R. A.; Hervés, P.; Liz-Marzán, L. M. Highly Catalytic Single-Crystal Dendritic Pt Nanostructures Supported on Carbon Nanotubes. *Chem. Mater.* **2009**, *21*, 1531−1535.
(24) Mahmoud, M. A.; Narayanan, R.; El-Sayed, M. A. Enhancing Colloidal Metallic Nanocatalysis: Sharp Edges and Corners for Solid Nanoparticles and Cage Effect for Hollow Ones. *Acc. Chem. Res.* **2013**, *46*, 1795−1805.
(25) Guo, S. J.; Li, J.; Dong, S. J.; Wang, E. K. Three-Dimensional Pt-on-Au Bimetallic Dendritic Nanoparticle: One-Step, High-Yield

Synthesis and Its Bifunctional Plasmonic and Catalytic Properties. *J. Phys. Chem. C* **2010**, *114*, 15337−15342.
(26) Hao, F.; Nehl, C. L.; Hafner, J. H.; Nordlander, P. Plasmon Resonances of a Gold Nanostar. *Nano Lett.* **2007**, *7*, 729−732.
(27) Rodríguez-Lorenzo, L.; Álvarez-Puebla, R. A.; Pastoriza-Santos, I.; Mazzucco, S.; Stéphan, O.; Kociak, M.; Liz-Marzán, L. M.; de Abajo, J. G.; Zeptomol, F. Detection Through Controlled Ultrasensitive Surface-Enhanced Raman Scattering. *J. Am. Chem. Soc.* **2008**, *130*, 4590−4591.
(28) Cheng, L. C.; Huang, J. H.; Chen, H. M.; Lai, T. C.; Yang, K. Y.; Liu, R. S.; Hsiao, M.; Chen, C. H.; Her, L. J.; Tsai, D. P. Seedless, Silver-Induced Synthesis of Star-Shaped Gold/Silver Bimetallic Nanoparticles as High Efficiency Photothermal Therapy Reagent. *J. Mater. Chem.* **2012**, *22*, 2244−2253.
(29) Navarro, J. R. G.; Liotta, A.; Faure, A. C.; Lerouge, F.; Chaput, F.; Micouin, G.; Baldeck, P. L.; Parola, S. Tuning Dye-to-Particle Interactions toward Luminescent Gold Nanostars. *Langmuir* **2013**, *29*, 10915−10921.
(30) Rodríguez-Lorenzo, L.; Álvarez-Puebla, R. A.; Pastoriza-Santos, I.; Mazzucco, S.; Stéphan, O.; Kociak, M.; Liz-Marzán, L. M.; de Abajo, F. J. G. Zeptomol Detection Through Controlled Ultrasensitive Surface-Enhanced Raman Scattering. *J. Am. Chem. Soc.* **2009**, *131*, 4616−4618.
(31) Wunder, S.; Polzer, F.; Lu, Y.; Mei, Y.; Ballauff, M. Kinetic Analysis of Catalytic Reduction of 4-Nitrophenol by Metallic Nanoparticles Immobilized in Spherical Polyelectrolyte Brushes. *J. Phys. Chem. C* **2010**, *114*, 8814−8820.
(32) Henglein, A.; Lilie, J. Storage of Electrons in Aqueous Solution: the Rates of Chemical Charging and Discharging the Colloidal Silver Microelectrode. *J. Am. Chem. Soc.* **1981**, *103*, 1059−1066.
(33) Chiu, C. Y.; Chung, P. J.; Lao, K. U.; Liao, C. W.; Huang, M. H. Facet-Dependent Catalytic Activity of Gold Nanocubes, Octahedra, and Rhombic Dodecahedra toward 4-Nitroaniline Reduction. *J. Phys. Chem. C* **2012**, *116*, 23757−23763.
(34) Ren, X. Q.; Tan, E. Z.; Lang, X. F.; You, T. T.; Jiang, L.; Zhang, H. Y.; Yin, P. G.; Guo, L. Observing Reduction of 4-Nitrobenzenthiol on Gold Nanoparticles in Situ using Surface-Enhanced Raman Spectroscopy. *Phys. Chem. Chem. Phys.* **2013**, *15*, 14196−14201.
(35) Kang, L. L.; Xu, P.; Zhang, B.; Tsai, H. H.; Han, X. J.; Wang, H. L. Laser Wavelength- and Power-Dependent Plasmon-Driven Chemical Reactions Monitored using Single Particle Surface Enhanced Raman Spectroscopy. *Chem. Commun.* **2013**, *49*, 3389−3391.
(36) Dong, B.; Fang, Y. R.; Chen, X. W.; Xu, H. X.; Sun, M. T. Substrate-, Wavelength-, and Time-Dependent Plasmon-Assisted Surface Catalysis Reaction of 4-Nitrobenzenethiol Dimerizing to *p*,*p*′-Dimercaptoazobenzene on Au, Ag, and Cu Films. *Langmuir* **2011**, *27*, 10677−10682.
(37) Huang, Y. F.; Zhu, H. P.; Liu, G. K.; Wu, D. Y.; Ren, B.; Tian, Z. Q. When the Signal Is Not from the Original Molecule To Be Detected: Chemical Transformation of *para*-Aminothiophenol on Ag during the SERS Measurement. *J. Am. Chem. Soc.* **2010**, *132*, 9244−9246.
(38) Skadtchenko, B. O.; Aroca, R. Surface-enhanced Raman Scattering of *p*-Nitrothiophenol Molecular Vibrations of its Silver Salt and the Surface Complex Formed on Silver Islands and Colloids. *Spectrochim. Acta, Part A* **2001**, *57*, 1009−1016.
(39) Cui, Q. L.; Yashchenok, A.; Zhang, L.; Li, L. D.; Masic, A.; Wienskol, G.; Möhwald, H.; Bargheer, M. Fabrication of Bifunctional Gold/Gelatin Hybrid Nanocomposites and Their Application. *ACS Appl. Mater. Interfaces* **2014**, *6*, 1999−2002.
(40) Wu, D. Y.; Zhao, L. B.; Liu, X. M.; Huang, R.; Huang, Y. F.; Ren, B.; Tian, Z. Q. Photon-Driven Charge Transfer and Photocatalysis of *p*-Aminothiophenol in Metal Nanogaps: a DFT Study of SERS. *Chem. Commun.* **2011**, *47*, 2520−2522.